Electronic Supplementary Material (ESI) for Dalton Transactions.

Supplementary Information

Electrophilic activation of alkynes promoted by a cationic alkylidene complex of Pt(II)

María M. Alcaide,[a] Práxedes Sánchez,[a] Eleuterio Álvarez,[a] Celia Maya,[a] Joaquín López-Serrano*,[a] Riccardo Peloso*[a]

Synthesis of new compounds

General considerations. All preparations and manipulations were carried out under oxygen free nitrogen using conventional Schlenk techniques. Solvents were rigorously dried and degassed before use. ^{1}H NMR, ^{13}C NMR, ^{31}P NMR spectra were recorded at 400 MHz, using the solvent peak as the internal reference. Compound **2** was prepared according to the literature.[1] Other chemicals were commercially available and used as received.

General procedure for the synthesis of complexes 3a-c. According to the literature,1 complex **1a** was generated *in situ* by adding dichloromethane (*ca.* 5 mL) to a solid mixture of **2** (47 mg, 0.10 mmol) and $[Ph_3C]^+[BF_4]^-$ (33 mg, 0.10 mmol) or $[Ph_3C]^+[PF_6]^-$ (39 mg, 0.10 mmol) at -60 °C. After 10 min stirring, the alkyne (0.10 mmol) was added by a syringe under a nitrogen flow and the mixture was allowed to reach the room temperature. Pure samples of compounds **3a-c** were obtained by evaporation of the volatiles, washing the solid residue with diethylether, and recrystallization of the crude from dichloromethane/diethylether solutions at 0 °C. Yield: 55-60%.

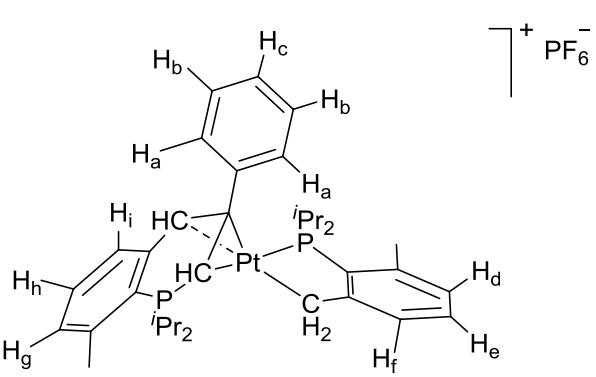

Compound 3a·PF_6. ^{1}H NMR (400 MHz, CD_2Cl_2): δ 7.51 (m, 2H, H_a), 7.47 (dd, 1H, $^{5}J_{PH}$ =1.2 Hz, H_h), 7.44 (d, 1H, H_c), 7.38 (t, 2H, H_b), 7.34 (dd, $^{4}J_{PH}$ = 3.7 Hz, H_i), 7.30 (d, 1H, H_f), 7.20 (br, 2H, H_e y H_g), 6.92 (dd, 1H, $^{4}J_{PH}$ = 3.0 Hz, H_d), 6.08 (br t, 1H, $^{4}J_{HH} \approx {}^{3}J_{PH} \approx$ 2.0 Hz, allyl C-CH-C), 4.30 (d, 1H, $^{2}J_{HH}$ = 16.3 Hz, $^{2}J_{PtH}$ = 102.8 Hz, C*H*H-Pt), 4.05 (d, 1H, $^{2}J_{HH}$ = 16.3 Hz, $^{2}J_{PtH}$ = 93.5 Hz, CH*H*-Pt), 3.73 (ddd, 1H, $^{4}J_{HH}$ = 2.0 Hz, $^{2}J_{PH}$ = 8.0 Hz, $^{3}J_{PH}$ = 5.0 Hz, $^{2}J_{PtH}$ =

[1] J. Campos, R. Peloso and E. Carmona, *Angew. Chem. Int. Ed.*, 2012, **51**, 8255-8258.

18.4 Hz, allyl C-CH-P), 3.13 (m, 1H, CH ^{i}Pr), 2.64 (m, 1H, CH ^{i}Pr), 2.54 (m, 2H, CH ^{i}Pr), 2.47 (s, 3H, CH_3 Xyl), 2.41 (s, 3H, CH_3 Xyl), 1.75 (dd, 3H, $^{3}J_{HH}$ = 6.9 Hz, $^{3}J_{PH}$ = 17.8 Hz, CH_3 ^{i}Pr), 1.42 (dd, 3H, $^{3}J_{HH}$ = 7 Hz, $^{3}J_{PH}$ = 16.6 Hz, CH_3 ^{i}Pr), 1.41 (dd, 3H, $^{3}J_{HH}$ = 7.24 Hz, $^{3}J_{PH}$ = 18.3 Hz, CH_3 ^{i}Pr), 1.02 (dd, 3H, $^{3}J_{HH}$ = 7 Hz, $^{3}J_{PH}$ = 18 Hz, CH_3 ^{i}Pr), 0.92 (m, 6H, CH_3 ^{i}Pr), 0.67 (dd, 3H, $^{3}J_{HH}$ = 7 Hz, $^{3}J_{PH}$ = 16.2 Hz, CH_3 ^{i}Pr) 0.22 (dd, 3H, $^{3}J_{HH}$ = 7 Hz, $^{3}J_{PH}$ = 17.9 Hz) ppm. All aromatic ^{3}J coupling constants are *ca.* 7-8 Hz.

$^{31}P\{^{1}H\}$ NMR (202.47 MHz, CD_2Cl_2): δ 81.1 (d, $^{3}J_{PP}$ = 14 Hz, $^{1}J_{PPt}$ = 3770 Hz), 37.7 (d, $^{3}J_{PP}$ = 14 Hz, $^{2}J_{PPt}$ = 80 Hz), -145.0 (sept, $^{1}J_{PF}$ = 711 Hz) ppm.

$^{13}C\{^{1}H\}$ NMR (125.78 MHz, CD_2Cl_2): δ 159.4 (d, $^{2}J_{CP}$ = 28 Hz, *C*CH_2Pt), 144.4 (d, J_{CP} = 4 Hz, aromatic C), 140.9 (d, $^{2}J_{CP}$ = 8 Hz, *C*CH_3 Xyl), 140.6 (d, J_{CP} = 3 Hz, aromatic C), 137.3 (d, J_{CP} = 7 Hz, aromatic C), 133.5 (d, $^{4}J_{CP}$ = 3 Hz, CH_e), 131.6 (d, $^{3}J_{CP}$ = 3 Hz, CH_f), 130.5 (s, CH_i), 130.4 (s,CH_b), 129.0 (s, CH_h), 128.8 (d, $^{3}J_{CP}$ = 6.7 Hz, CH_a), 127.5 (d, $^{3}J_{CP}$ = 8.8 Hz, CH_d), 127.0 (d, $^{3}J_{CP}$ = 13 Hz, CH_c), 126.4 (virtual t, $^{3+6}J_{CP}$ = 10 Hz, CH_g), 115.2 (s, aromatic C), 107.6 (s, aromatic C), 107.0 (s, allyl *C*-Ph), 72.1 (d, $^{1}J_{CPt}$ = 24 Hz, $^{2}J_{CP}$ = 8 Hz, allyl C-*C*H-C), 30.3 (dd, $^{1}J_{CP}$ = 40 Hz, $^{4}J_{CP}$ = 5 Hz, CH^{i}Pr), 28.7 (d, $^{1}J_{CP}$ = 31 Hz, CH^{i}Pr), 27.7 (dd, $^{1}J_{CP}$ = 64 Hz, $^{2}J_{CP}$ = 46 Hz, allyl C-*C*H-P), 24.8 (d, $^{1}J_{CP}$ = 29 Hz, CH^{i}Pr), 21.9 (d, $^{3}J_{CP}$ = 4 Hz, CH_3Xyl), 21.7 (s, CH_3Xyl), 20.4-19.6 (m, $CH_3{}^{i}$Pr), 18.2 (m, $CH_3{}^{i}$Pr), 17.1 (d, $CH_3{}^{i}$Pr), 15.9 (s, $CH_3{}^{i}$Pr) ppm. Resonance of the CH_2 cabon nucleus masked by other aliphatic signals.

Anal. Calc. for $C_{36}H_{49}F_6P_3Pt$: C, 48.93; H, 5.59. Found: C, 49.3; H, 5.6 %.

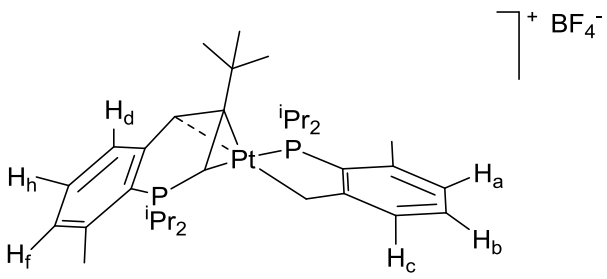

Compound 3b·BF_4. ^{1}H NMR (400 MHz, CD_2Cl_2): δ 7.36 (t, 1H, $^{3}J_{HH}$ = 7.8 Hz, H_h), 7.25-7.16 (m, 3H, H_c,H_b, H_f), 7.07 (dd, 1H, $^{3}J_{HH}$ = 7.8 Hz, $^{4}J_{PH}$ = 3.7 Hz, H_d), 6.89 (br d, 1H, $^{3}J_{HH}$ = 7.4 Hz, H_a), 5.73 (br s, 1H, allyl C-CH-C), 4.16 (d, 1H, $^{2}J_{HH}$ = 16.2 Hz, $^{2}J_{PtH}$ = 92.0 Hz, C*H*H-Pt), 3.88 (br dd, 1H, $^{2}J_{PH}$ = 8.3 Hz, $^{3}J_{PH}$ = 5.6 Hz, $^{2}J_{PtH}$ = 19.6 Hz, allylic C-CH-P), 3.71 (d, 1H, $^{2}J_{HH}$ = 16.2 Hz, $^{2}J_{PtH}$ = 99.5 Hz, CH*H*-Pt),

3.35 (apparent oct, 1H, $^{3}J_{PH}$ = 7.2 Hz, $^{3}J_{HH}$ = 7.1 Hz, CH^{i}Pr), 2.90-2.76 (m, 2H, CH^{i}Pr), 2.51-2.40 (m, 7H, CH_3 Xyl and CH^{i}Pr), 1.70 (dd, 3H, $^{3}J_{HH}$ = 6.9 Hz, $^{3}J_{PH}$ = 18.0 Hz, CH_3 ^{i}Pr), 1.56 (dd, 3H, $^{3}J_{HH}$ = 6.9 Hz, $^{3}J_{PH}$ = 17.0 Hz, CH_3^{i}Pr), 1.45 (dd, 3H, $^{3}J_{HH}$ = 7.0 Hz, $^{3}J_{PH}$ = 17.8 Hz, CH_3^{i}Pr), 1.40 (dd, 3H, $^{3}J_{HH}$ = 6.9 Hz, $^{3}J_{PH}$ = 19.0 Hz, CH_3^{i}Pr), 1.29 (s, 9H, CH_3^{t}Bu), 1.0 (dd, 3H, $^{3}J_{HH}$ = 6.9 Hz, $^{3}J_{PH}$ = 18.7 Hz, CH_3^{i}Pr), 0.93 (dd, 3H, $^{3}J_{HH}$ = 7.2 Hz, $^{3}J_{PH}$ = 18.1 Hz, CH_3^{i}Pr), 0.73 (dd, 3H, $^{3}J_{HH}$ = 7.0 Hz, $^{3}J_{PH}$ = 19.0 Hz, CH_3^{i}Pr), 0.68 (dd, 3H, $^{3}J_{HH}$ = 6.90 Hz, $^{3}J_{PH}$ = 18.0 Hz, CH_3^{i}Pr) ppm.

^{31}P{^{1}H} NMR (202.47 MHz, $CDCl_3$) δ 77.4 (d, $^{3}J_{PP}$ = 15 Hz, $^{1}J_{PPt}$ = 3846 Hz), 36.8 (d, $^{3}J_{PP}$ = 15 Hz, $^{2}J_{PPt}$ = 90 Hz) ppm.

^{13}C{^{1}H} NMR (125.78 MHz, $CDCl_3$) δ 159.8 (d, $^{2}J_{CP}$ = 28 Hz, *C*CH_2Pt), 146.9 (s, aromatic C), 144.6 (d, $^{2}J_{CP}$ = 4 Hz, J_{CPt} = 28 Hz, C aromático), 143.9 (s, aromatic C), 141.2 (d, $^{2}J_{CP}$ = 8 Hz, *C*CH_3 Xyl), 140.3 (d, J_{CP} = 3, aromatic C), 133.0 (d, $^{4}J_{CP}$ = 2 Hz, CH_h), 131.6 (d, $^{3}J_{CP}$ = 2 Hz, CH_f), 129.5 (s, CH_b), 128.3 (s, CH_a), 128.0 (s, CH_c), 126.9 (d, $^{3}J_{CP}$ = 8 Hz, H_d), 70.1 (d, $^{2}J_{CP}$ = 8 Hz allylic CH-P), 36.9 (d, $^{3}J_{CP}$ = 5 Hz, allylic *C*^{t}Bu), 30.4-29.4 (m, CH_3^{t}Bu), 29.9 (s, allylic CH), 28.2 (d, J_{CP} = 30 Hz CH^{i}Pr), 26.47 (d, J_{CP} = 23 Hz, CH^{i}Pr), 26.0 (d, J_{CP} = 44 Hz CH^{i}Pr), 22.2 (d, $^{3}J_{CP}$ = 3 Hz, CH_3Xyl), 20.3-19.4 (m, CH_3^{i}Pr), 19.2 (d, $^{2}J_{CP}$ = 2, $^{1}J_{PtC}$ = 18 Hz, CH_2Pt), 18.9 (d, $^{2}J_{CP}$ = 41 Hz, CH^{i}Pr), 18.7 (s, C^{t}Bu), 17.5-17.3 (m, CH_3^{i}Pr), 16.5 (s, CH_3^{i}Pr).

Anal. Calc. for $C_{34}H_{53}BF_4P_2Pt$: C, 50.69; H, 6.63. Found: C, 50.9; H, 6.4 %.

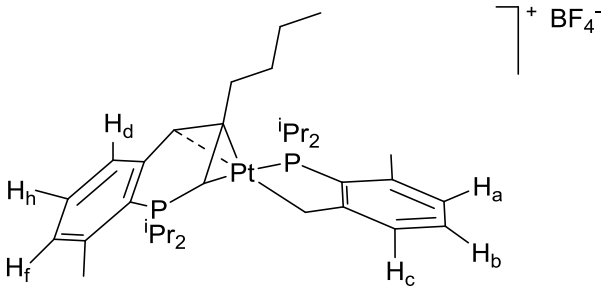

Compound 3c·BF_4. ^{1}H NMR (400 MHz, CD_2Cl_2): δ 7.36 (t, 1H, $^{3}J_{HH}$ = 7.9 Hz, H_h), 7.25-7.16 (m, 3H, H_c,H_b, H_f), 7.05 (dd, 1H, $^{3}J_{HH}$ = 7.4 Hz, $^{4}J_{PH}$ = 3.3 Hz, H_d), 6.89 (br d, 1H, $^{3}J_{HH}$ = 7.0 Hz, H_a), 5.60 (br s, 1H, allylic C-CH-C), 4.12 (d, 1H, $^{2}J_{HH}$ = 14.7 Hz, $^{2}J_{PtH}$ = 99.7 Hz, C*H*H-Pt), 3.81 (d, 1H, $^{2}J_{HH}$ = 16.3 Hz, $^{2}J_{PtH}$ = 96.8 Hz, CH*H*-Pt), 3.65 (br dd, 1H, $^{2}J_{PH}$ = 9.2 Hz, $^{3}J_{PH}$ = 5.5 Hz, $^{2}J_{PtH}$ = 22.1 Hz, allylic C-CH-P), 3.25 (app oct, 1H, $^{3}J_{PH}$ = 6.4 Hz, $^{3}J_{HH}$ = 6.7 Hz, CH^{i}Pr), 3.12-2.94 (m, 1H, CH^{i}Pr), 2.78 (app oct,

2H, $^{3}J_{PH}$ = 6.5 Hz, $^{3}J_{HH}$ = 7.3 Hz, CH^{i}Pr), 2.45 (br s, 6H, CH_3Xyl), 1.69 (dd, 3H, $^{3}J_{HH}$ = 7.1 Hz, $^{3}J_{PH}$ = 18.2 Hz, CH_3^{i}Pr), 1.53 (dd, 3H, $^{3}J_{HH}$ = 6.5 Hz, $^{3}J_{PH}$ = 16.8 Hz, CH_3^{i}Pr), , 1.33 (dd, 3H, $^{3}J_{HH}$ = 7.1 Hz, $^{3}J_{PH}$ = 18.1 Hz, CH_3^{i}Pr), 1.10 (dd, 3H, $^{3}J_{HH}$ = 6.9 Hz, $^{3}J_{PH}$ = 18.4 Hz, CH_3^{i}Pr), 1.06 (dd, 3H, $^{3}J_{HH}$ = 7.0 Hz, $^{3}J_{PH}$ = 18.0 Hz, CH_3^{i}Pr), 0.99 (dd, 3H, $^{3}J_{HH}$ = 7.1 Hz, $^{3}J_{PH}$ = 18.1 Hz, CH_3^{i}Pr), 0.91 (t, 3H, $^{2}J_{HH}$ = 7.4 Hz, CH_3Hexine), 0.83 (dd, 3H, $^{3}J_{HH}$ = 6.9 Hz, $^{3}J_{PH}$ = 17.8 Hz, CH_3^{i}Pr), 0.74 (dd, 3H, $^{3}J_{HH}$ = 6.9 Hz, $^{3}J_{PH}$ = 17.8 Hz, CH_3^{i}Pr), 0.65 (dd, 3H, $^{3}J_{HH}$ = 7.1 Hz, $^{3}J_{PH}$ = 17.0 Hz, CH_3^{i}Pr) ppm.

^{31}P{^{1}H} NMR (202.47 MHz, $CDCl_3$): δ 79.7 (d, $^{3}J_{PP}$ = 15 Hz, $^{1}J_{PPt}$ = 3807 Hz), 36.5 (d, $^{3}J_{PP}$ = 5 Hz, $^{2}J_{PPt}$ = 84 Hz) ppm.

^{13}C{^{1}H} NMR (125.78 MHz, $CDCl_3$): δ 159.8 (d, $^{2}J_{CP}$ = 28 Hz, *C*CH_2Pt), 146.9 (s, aromatic C), 144.2 (d, $^{2}J_{CP}$ = 3 Hz, J_{CPt} = 25 Hz, aromatic C), 144.0 (s, aromatic C), 141.3 (d, $^{2}J_{CP}$ = 9 Hz, *C*CH_3Xyl), 140.2 (d, J_{CP} = 3 Hz, aromatic C), 133.1 (d, $^{4}J_{CP}$ = 2 Hz, CH_h), 131.7 (d, $^{3}J_{CP}$ = 2 Hz, CH_f), 129.5 (s br, CH_b), 128.3 (s br, CH_a), 127.9 (s br, CH_c), 126.6 (d, $^{3}J_{CP}$ = 8 Hz, H_d), 74.2 (d, $^{1}J_{CP}$ = 7 Hz, allylic CH-P), 39.5 (d, $^{3}J_{CP}$ = 5 Hz, allylic C-hexine), 30.4-29.5 (m, CH_2Hexine + allylic CH), 28.6 (d, $^{2}J_{CP}$ = 30 Hz CH^{i}Pr), 25.5 (d, $^{2}J_{CP}$ = 22 Hz, CH^{i}Pr), 25.3 (d, $^{2}J_{CP}$ = 41 Hz CH^{i}Pr), 22.1 (s br, CH_3Xyl), 20.7-19.9 (m, CH_3^{i}Pr), 19.6 (d, $^{2}J_{CP}$ = 2, $^{1}J_{PtC}$ = 19 Hz, CH_2Pt), 18.9 (d, $^{2}J_{CP}$ = 40 Hz, CH^{i}Pr), 17.6-17.2 (m, CH_3^{i}Pr), 16.5 (s, CH_3^{i}Pr), 13.8 (s, CH_3Hexine).

Anal. Calc. for $C_{34}H_{53}BF_4P_2Pt$: C, 50.69; H, 6.63. Found: C, 60.0; H, 6.5 %.

Computational studies

Computational Details. Calculation of the geometries of all complexes were performed with Gaussian 09 without geometry constrains.[2] The nature of the optimized geometries as local minima or saddle points (transition states) was characterised by vibrational analysis. The local minima connected by a given transition state were determined by IRC calculations or by optimizing two geometries resulting from allowing the molecule to vibrate along the imaginary frequency at said TS. The basis set 6-31g(d,p),[3] including polarization functions, has been used for all atoms, except for Pt, which was described with the SDD basis and its associated electron core potential.[4] These basis sets were used in combination with the Head Gordon functional ωB97XD[5] with empirical dispersion corrections.[6] Bulk solvent effects (dichloromethane) were included during optimization with the SMD continuum model.[7] Orbital localization (Foster Boys),[8] as well as calculation of the positions of the orbitals' centroid was carried out with Gaussian09 and the Multiwfn[9] code. NBO analysis was carried out with the NBO6.0 program.[10] The Cylview 1.0[11] and VMD 1.9.3[12] codes were used for rendering and animation of optimized geometries, orbitals, and centroids.

---

[2] Gaussian 09, Revisions B.01 and E.01, M. J. Frisch, G. W. Trucks, H. B. Schlegel, G. E. Scuseria, M. A. Robb, J. R. Cheeseman, G. Scalmani, V. Barone, G. A. Petersson, H. Nakatsuji, X. Li, M. Caricato, A. Marenich, J. Bloino, B. G. Janesko, R. Gomperts, B. Mennucci, H. P. Hratchian, J. V. Ortiz, A. F. Izmaylov, J. L. Sonnenberg, D. Williams-Young, F. Ding, F. Lipparini, F. Egidi, J. Goings, B. Peng, A. Petrone, T. Henderson, D. Ranasinghe, V. G. Zakrzewski, J. Gao, N. Rega, G. Zheng, W. Liang, M. Hada, M. Ehara, K. Toyota, R. Fukuda, J. Hasegawa, M. Ishida, T. Nakajima, Y. Honda, O. Kitao, H. Nakai, T. Vreven, K. Throssell, J. A. Montgomery, Jr., J. E. Peralta, F. Ogliaro, M. Bearpark, J. J. Heyd, E. Brothers, K. N. Kudin, V. N. Staroverov, T. Keith, R. Kobayashi, J. Normand, K. Raghavachari, A. Rendell, J. C. Burant, S. S. Iyengar, J. Tomasi, M. Cossi, J. M. Millam, M. Klene, C. Adamo, R. Cammi, J. W. Ochterski, R. L. Martin, K. Morokuma, O. Farkas, J. B. Foresman and D. J. Fox, Gaussian, Inc., Wallingford CT, 2010.

[3] (a) R. Ditchfield, W. J. Hehre and J. A. Pople , *J. Chem. Phys.* **1971**, *54*, 724-728; (b) W. J. Hehre, R. Ditchfield and J. A. Pople *J. Chem. Phys.* **1972**, *56*, 2257-2261; (c) P. C. Hariharan and J. A. Pople, *Theor. Chim. Acta* **1973**, *28*, 213-222; (d) M. M. Francl, W. J. Pietro, W. J. Hehre, J. S. Binkley, M. S. Gordon, D. J. DeFrees and J. A. Pople, *J. Chem. Phys.* **1982**, *77*, 3654-3665.

[4] D. Andrae, U. Haeussermann, M. Dolg, H. Stoll and H. Preuss, *Theor. Chim. Acta* **1990**, *77*, 123-141.

[5] J.-D. Chai and M. Head-Gordon, *Phys. Chem. Chem. Phys.* **2008**, *10*, 6615-6620.

[6] S. Grimme, *J. Comp. Chem* **2006**, *27*, 1787-1799.

[7] A. V. Marenich, C. J. Cramer and D. G. Truhlar, *J. Phys. Chem. B* **2009**, *113*, 6378–6396.

[8] (a) S. F. Boys, *Rev. Mod. Phys.* **1960**, *32*, 296-299; (b) J. M. Foster and S. F. Boys, *Rev. Mod. Phys.* **1960**, *32*, 300-302.

[9] (a) Multiwfn, v. 6.0. http://sobereva.com/multiwfn/; (b) T. Lu and F. Chen, *J. Comput. Chem.* **2012**, *33*, 580-592.

[10] (a) E. D. Glendening, C. R. Landis and F. Weinhold, *J. Comput. Chem.* **2013**, *34*, 1429-1437; (b) E. D. Glendening, J. K. Badenhoop, A. E. Reed, J. E. Carpenter, J. A. Bohmann, C. M. Morales, C. R. Landis and F. Weinhold, NBO 6.0.; Theoretical Chemistry Institute, University of Wisconsin: Madison, **2013**.

[11] C. Y. Legault, CYLview, 1.0b;, Université de Sherbrooke, **2009**.

[12] W. Humphrey, A. Dalke and K. Schulten, *J. Molec. Graphics,* **1996**, *14*, 33-38. The VMD software can be downloaded from https://www.ks.uiuc.edu/Research/vmd/.

Full energy profile for the formation of 3a and $3a_R$. In addition to the intermediates discussed in the main text, Figure S1 includes the energies for the adduct **1a**·phenylacetylene, and **A'**, a rotamer of **A**, leading (as indicated by relaxed Potential Energy Surface Scans) to **B**. Also included is the profile for the formation of $3a_R$ from B_R. We could not locate an intermediate, isomer of **A** resulting from attack of the ≡CPh terminus of the alkyne to the alkylidenic carbon.

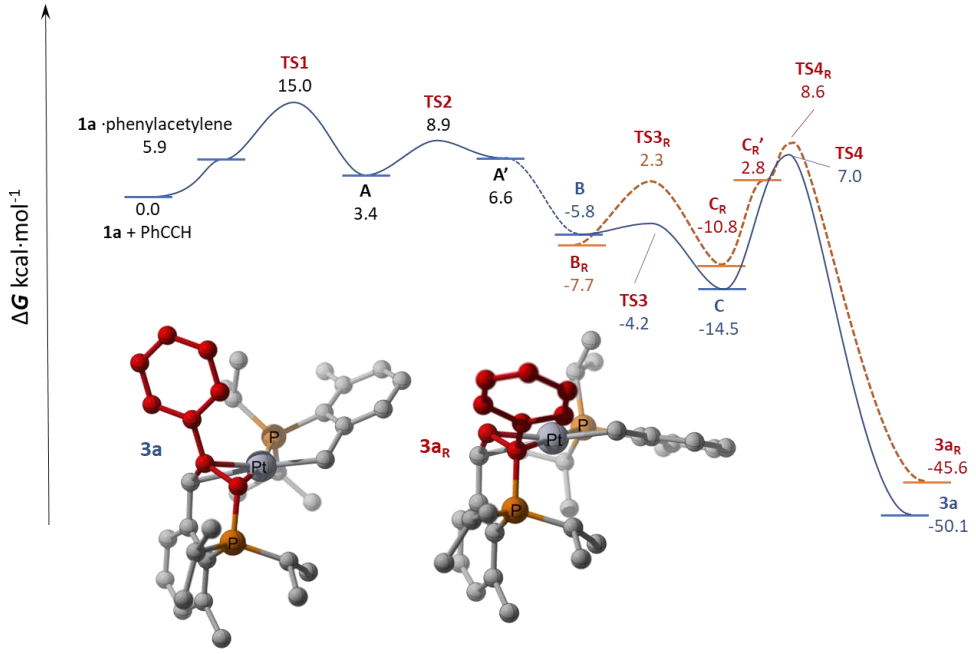

Figure S1. Full energy profile for the formation of **3a** from **1a**, including the path for the formation of the isomer $3a_R$ from B_R. The inset shows the optimized geometry of $3a_R$ with the fragment originating in the alkyne.

Localized orbitals analysis and orbital population evolution. We followed the evolution of the centroids of relevant localized orbitals (Foster-Boys) for the intermolecular nucleophilic attack of diphenylacetylene to the carbenic carbon of **1a**. To do so, we employed the method described by Vidossich and Lledós.[13] This method yields a description of electron evolution along a reaction path similar to that of the pushing arrow method used in organic chemistry. Thus, we performed single point calculations for selected geometries along the IRC path in *forward* and *backward* directions starting from **TS1**. Localization of these wavefunctions with the Foster-Boys scheme was followed by visual inspection of the resulting orbitals to find those relevant to the nucleophilic attack of the alkyne and location of their centroids. Figure S2 (below) shows one π orbital (and its corresponding centroid as a red dot) of the C≡C bond before any significant interaction has occurred with the carbenic carbon (below, left) and the evolution of such orbital after **TS1** into an incipient σ C—C bond (below, right). The upper part of the figure exhibits the evolution of the position of the centroid of said orbital along the IRC path (the arrow indicates the *direction* of the transformation). Also shown, the evolution of the centroid of the orbital for the σ Pt—C interaction with the carbenic carbon reveals that this orbital increases its carbon character as the C—C bond formation progresses. In addition, the bond indices (Mayer)[14] for bonds involved in the nucleophilic attack were calculated along the IRC path. As can be seen in Figure S2, the bond index for the C≡C bond decreases from more than 2.5 to ca. 2, while the new C—C bond increases its bond index from nearly zero to ca. 1. Finally, the bond index for the Pt=C bond, decreases. This can be interpreted in part as a decrease of the multiple bond character of this bond (see the NBO analysis below).

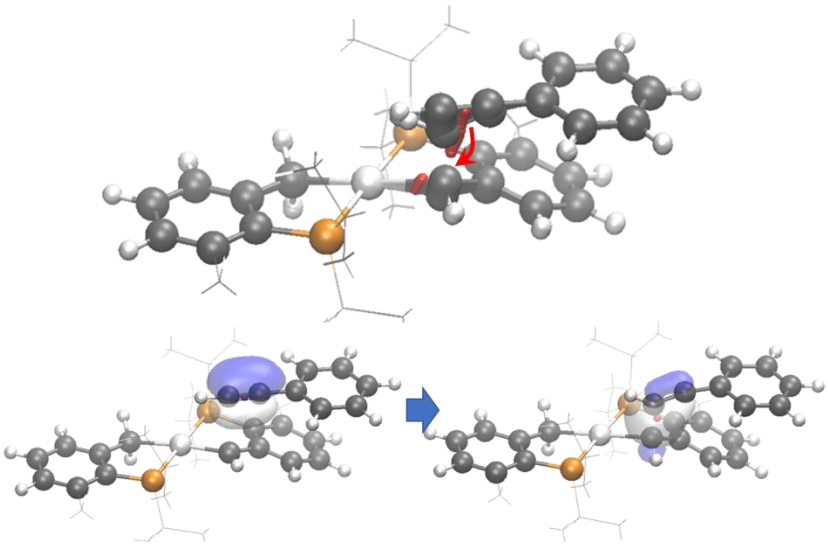

Figure S2. Evolution of the centroids (upper figure, red dots) of one C≡C π orbital, and the σ-Pt—C orbital along the IRC during the nucleophilic attack of the terminal carbon atom of the alkyne to the

[13] P. Vidossich and A. Lledós, *Dalton Trans.* **2014**, *43*, 11145-11151.
[14] I. Mayer, *Chem. Phys. Lett.* **1983**, ***97***, 270-274.

carbenic carbon of **1a**. The figures below illustrate the transformation of the C≡C π orbital (0.05 a.u. isosurface) to yield a new C—C bond.

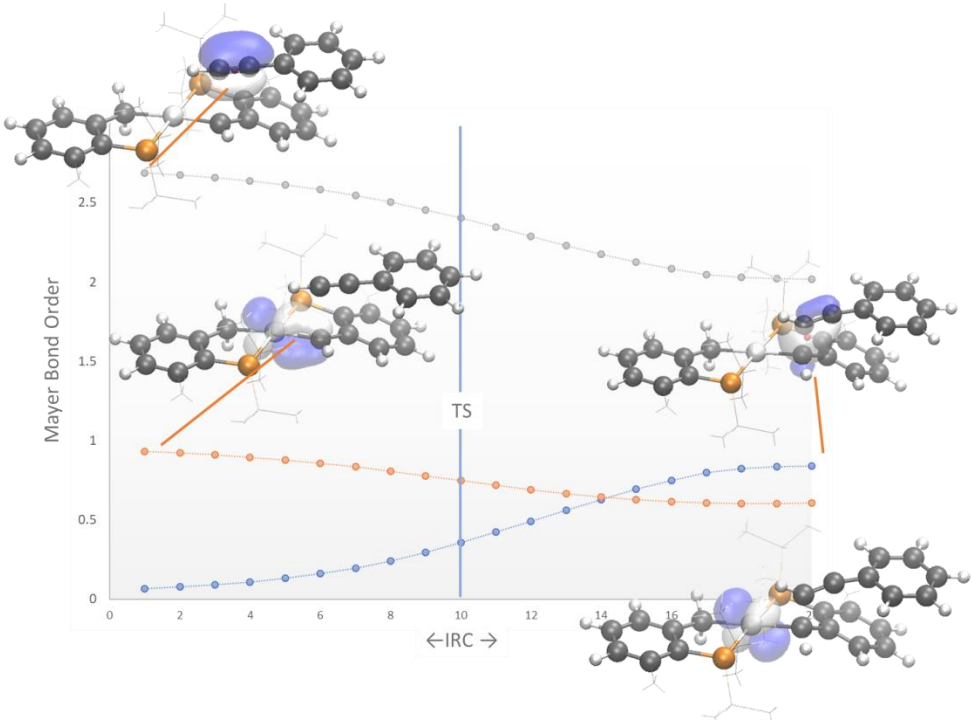

Figure S3. Evolution of the Mayer Bond Indices along the intrinsic reaction coordinate for relevant bonds. A vertical bar shows the position of **TS1**. Four superimposed figures show molecular geometries at a given point along the IRC path with relevant localized orbitals (Foster-Boys) contributing to a given bond and their centroids (in red). The bottom left figure shows the Pt-localized d orbital previously involved in the stabilization of the alkylidene.

NBO analysis. NBO analysis was performed for **TS1** and **1a**·phenylacetylene, the *adduct* that *precedes* **TS1** along the reaction coordinate. Figure S4 shows the numbering scheme used in the following discussion. Tables S1-S4 summarize these results. At **TS1**, The C(5)—Pt—C(4) linkage is described as a 3c-4e *hyperbond*, with the preferred Lewis-like form being C(5)—Pt :C(4), i.e.: the Pt-alkyl bond is described as a 2c-2e bond, whereas the Pt-alkylidene σ interaction is described in terms of donation from a sp orbital located on C(4) onto the Pt—C(5) antibonding orbital (Table S1, entries 4 and 14; Table S2, entry 2). The Natural Localized Molecular Orbital (NLMO) corresponding to the donor sp NBO has 74.4 % and 13.2 % carbon/platinum contributions (Table S1, entry 5). The Pt—C(4) linkage is completed with donation form one d orbital on the platinum onto the *empty* p orbital (*lone vacancy* in the NBO terminology) located on the carbon, which accounts for the π interaction (Table S2, entry 1). This time the corresponding NLMO has 4.7% and 92.7% carbon/platinum contributions (Table S1, entry 4). Further stabilization of the alkylidenic carbon comes from donation from the π electron density of the adjacent aryl (Table S2, entry 3). The *delocalization energies* (E_{ij}, from second order perturbation theory analysis of the Fock

matrix) for these interactions are 42.5 and 65.0 kcal·mol^{-1} for the Pt and Aryl contributions, respectively. At the TS, the interaction between the alkyne and the alkylidenic carbon is described in term of electron donation from one π orbital of the alkyne's C≡C bond to the empty p orbital on C(4) (Table SC2, entry 4) with an associated delocalization energy E_{ij} = 134.6 kcal·mol^{-1}. A secondary, much weaker interaction (E_{ij} = 14.2 kcal·mol^{-1}) between the alkyne and the metal complex is also described as donation of electron density from the sp orbital on C(4) (effectively taking part in the σ-Pt—C(4) bond) to one π* (antibonding) C(43)≡C(44) orbital (Table S2, entry 2).

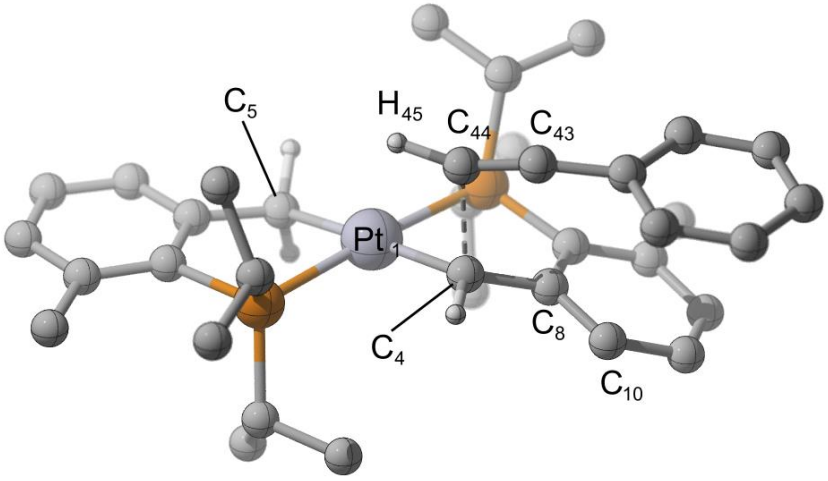

Figure S4. Optimized geometry of **TS1** with the numbering scheme used in the NBO discussion (most hydrogens omitted for clarity).

Table S1. Selected NBOs and corresponding **NLMOs for **TS1**

Entry	NBO	Occupation (e^-)	Composition	NLMO (description)	Parent NBO (%)	Composition (%)
1	†LP1 Pt	1.98	d (96.9%)	-	-	-
2	LP2 Pt	1.95	d (99.9%)	-	-	-
3	LP3 Pt	1.95	d (99.9%)	-	-	-
4	LP4 Pt	**1.87**	d (99.9%)	***Pt***=***C***H bond, **π**	92.7	92.7 Pt, 4.7 C(4), 1.4 C(44)
5	LP C(4) (alkylidene)	**1.51**	$sp^{1.11}$	***Pt***=***C***H bond, **σ**	74.4	13.2 Pt, 74.4 C(4) 7.83 C(5)
6	‡BD Pt—C(5) (alkyl)	1.90	$0.60sd^{1.55} + 0.80sp^{3.63}$	-	-	-
7	BD C(4)—C(8) (alkylidene)	1.98	$0.69sp^{1.85} + 0.72sp^{2.15}$	-	-	-
8	BD C(8)=C(10) (π bond)	**1.62**	0.72p+0.69p	Stabilization of the alkylidene by the aryl.	80.4	42.7 C(8), 37.7 C(10), 6.0 C(4)
9	BD C(43)≡C(44) (σ bond)	1.98	$0.71sp^{0.93} + 0.70sp^{1.18}$	-	-	-
10	BD C(43)≡C(44) (π bond)	1.98	0.71p+0.71p	-	-	-
11	BD C(43)≡C(44) (π bond)	**1.65**	0.67p + 0.74p	Nucleophilic attack of the alkyne to the alkylidene.	79.8	17.5 C(4), 33.5 C(43), 46.4 C(44)
12	BD ≡C(44)—H	1.97	$0.81sp^{1.05} + 0.58s$	-	-	-
13	*LV =C(4) (alkylidene)	**0.60**	p (98.4%)	-	-	-
14	††BD* Pt—C(5)	**0.48**	$0.8sd^{1.55} - 0.6sp^{3.63}$			
15	BD* C(43)≡C(44), π*	**0.16**	0.74p - 0.67p	-	-	-

**Only NLMOs from low occupancy NBOs or from filled NBOs with significant delocalization onto *empty* NBOs; †Lone Pair (located on one atom); ‡ Bonding orbital; **Lone valence* (*empty* orbital located on one atom); ††Antibonding orbital (*empty*).

Table S2. Selected donor-acceptor interactions in **TS1**

Entry	Donor NBO	Acceptor NBO	E_{ij} (kcal·mol^{-1})
1	[†]LP4 Pt	*LV =C(4) (alkylidene)	42.5
2	LP C(4) (alkylidene)	[††]BD* C(43)≡C(44)	14.2
		BD* Pt—C(5)	305.7
3	[‡]BD C(8)=C(10) (π bond)	*LV =C(4) (alkylidene)	65.0
4	BD C(43)≡C(44) (π bond)	*LV =C(4) (alkylidene)	134.6

[†]Lone Pair (located on one atom); [‡] Bonding orbital; **Lone valence* (*empty* orbital located on one atom); [††]Antibonding orbital (*empty*)

The results of the analogous analysis for **1a·phenylacetylene'** are summarized in Tables S3 and S4 and the numbering scheme used is the same as that for **TS1** (Figure S5).

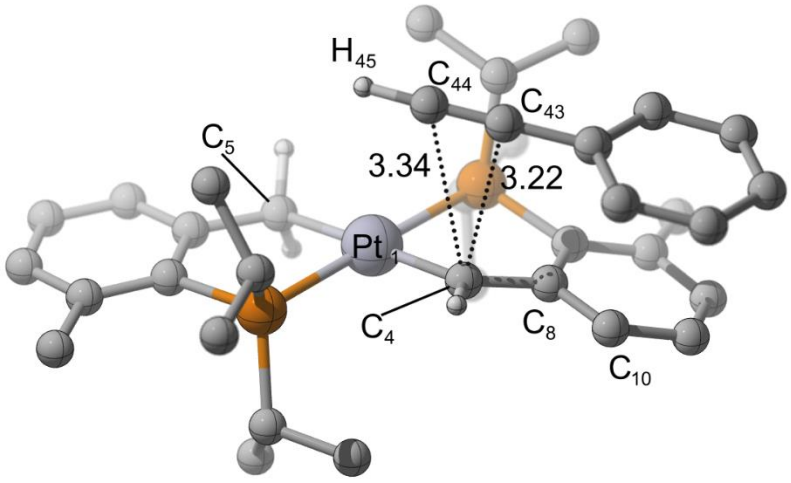

Figure S5. Optimized geometry of **1a·phenylacetylene'** with the numbering scheme used in the NBO discussion (most hydrogens omitted for clarity, C···C distances in Å).

This *adduct* features a shortest alkyne···**1a** contact of 3.22 Å between C(4) and C(43), compared to the C(4)···C(44) of 2.09 Å in **TS1** and, as expected, no interaction is found between the metal complex and alkyne fragments of **1a·phenylacetylene'**. In addition, the alkylidenic carbon is stabilized by π electron density donation from one d orbital on the platinum and from the electron density of the adjacent aryl onto its p orbital. But, compared with the situation in **TS1**, the delocalization energies are higher (Tables S3 and S4, entries 1 and 3). Also, the composition of the NLMO accounting for the Pt—

C(4) π interaction has higher carbon character, 13.5 % than at **TS1**, with only 4.7%. This is consistent with the decrease in the Pt—C(4) bond order upon nucleophilic attack of the alkyne described before.

Table S3. Selected NBOs and corresponding **NLMOs for **1a·phenylacetylene'**.

Entry	NBO	Occupation (e^-)	Composition	NLMO (description)	Parent NBO (%)	Composition (%)
1	†LP1 Pt	1.98	d (97.0%)	-	-	-
2	LP2 Pt	1.96	d (100.0%)	-	-	-
3	LP3 Pt	1.95	d (100.0%)	-	-	-
4	LP4 Pt	**1.74**	d (100.0%)	***Pt***=***C***H bond, **π**	85.2	85.2 Pt, **13.5** C(4)
5	‡BD Pt—C(4) (alkylidene)	1.92	$0.57sd^{1.40} + 0.82sp^{1.91}$	***Pt***=***C***H bond, **σ**	96.0	33.1 Pt, 64.2 C(4)
6	LP C(5) (alkyl)	**1.43**	$sp^{3.49}$	***Pt-C***H_2 bond, **σ**	70.1	17.2 Pt, 70.1 C(4)
6						
7	BD C(4)—C(8) (alkylidene)	1.98	$0.68sp^{1.79} + 0.73sp^{2.09}$	-	-	-
8	BD C(8)=C(10) (π bond)	**1.56**	0.75p+0.67p	Stabilization of the alkylidene by the aryl.	77.7	45.7 C(8), 32.4 C(10), 8.5 C(4)
9	BD C(43)≡C(44) (σ bond)	1.98	$0.72sp^{0.92} + 0.70sp^{0.91}$	-	-	-
10	BD C(43)≡C(44) (π bond)	1.98	0.71p+0.70p	-	-	-
11	BD C(43)≡C(44) (π bond)	1.94	0.71p + 0.70p	-	-	-
12	BD ≡C(44)—H	1.99	$0.80sp^{1.10} + 0.60s$	-	-	-
13	*LV =C(4) (alkylidene)	**0.51**	p (100.0%)	-	-	-
14	††BD* Pt—C(4)	**0.56**	$0.82sd^{1.40} - 0.57sp^{1.91}$			
15	BD* C(43)≡C(44), π*	None > 0.02	-	-	-	-

**Only NLMOs from low occupancy NBOs or from filled NBOs with significant delocalization onto *empty* NBOs; †Lone Pair (located on one atom); ‡ Bonding orbital; **Lone valence* (*empty* orbital located on one atom); ††Antibonding orbital (*empty*).

Table S4. Selected donor-acceptor interactions in **1a·phenylacetylene'**.

Entry	Donor NBO	Acceptor NBO	E_{ij} (kcal·mol^{-1})
1	[†]LP4 Pt	*LV(1) =C(4) (alkylidene)	77.8
2	LP C(5) (alkyl)	[††]BD* Pt—C(4)	288.9
3	[‡]BD C(8)=C(10) (π bond)	*LV(1) =C(4) (alkylidene)	94.2
4	BD C(43)≡C(44) (π bond)	*LV(1) =C(4) (alkylidene)	-

[†]Lone Pair (located on one atom); [‡] Bonding orbital; **Lone valence* (*empty* orbital located on one atom); [††]Antibonding orbital (*empty*).

Table S5. Wiberg bond indices.

	Pt—C(4) alkylidene	Pt—C(5) alkyl	C(43)≡C(44)	C(44)···C(4)
1a·phenylace	0.7671	0.4489	2.8184	0.0117
TS1	0.5208	0.4897	2.4794	0.3604

Table S6. Partial charges (e) in **1a·phenylacetylene'**

	Pt	C(4) alkylidene
NBO	0.330	-0.198
Mulliken	-0.510	-0.216
APT	-0.773	1.238
Hirshfeld	0.141	-0.019
Lowdin	-1.70964549	0.12338955

X-Ray diffraction analyses

Crystals of suitable size for X-ray diffraction analysis of **3a**, **3b** and **3c** were coated with dry perfluoropolyether and mounted on glass fibres and fixed in a cold nitrogen stream (T = 213 K) to the goniometer head. Data collection was performed on a Bruker-Nonius X8Apex-II CCD diffractometer, using monochromatic radiation λ(Mo K_α) = 0.71073 Å, by means of ω and ϕ scans with a width of 0.50 degree. The data were reduced (SAINT)[15] and corrected for absorption effects by the multi-scan method (SADABS).[16] The structures were solved by direct methods (SIR-2002)[17] and refined against all F^2 data by full-matrix least-squares techniques (SHELXL-2016/6 or SHELXL-2018/3)[18] minimizing $w[F_o^2-F_c^2]^2$. All non-hydrogen atoms were refined anisotropically. The hydrogen atoms were included from calculated positions and refined riding on their respective carbon atoms with isotropic displacement parameters. A summary of cell parameters, data collection, structure solution, and refinement for these two crystal structures are given bellow. The corresponding crystallographic data were deposited with the Cambridge Crystallographic Data Centre as supplementary publications. CCDC 2126369 **(3a),** 21263670 (**3b**) and 2126371 **(3c)**. The data can be obtained free of charge *via* https://www.ccdc.cam.ac.uk/structures/.

[15] Bruker. SAINT. *APEX2* **2007**, Bruker AXS Inc., Madison, Wisconsin, USA.
[16] (a) G. M. Sheldrick, SADABS, Programs for Scaling and Absorption Correction of Area Detector Data. *SADABS, Programs Scaling Absorpt. Correct. Area Detect. Data* **1997**, University of Göttingen: Göttingen, Germany; (b) Bruker. SADABS. *APEX2* **2007**, Bruker AXS Inc., Madison, Wisconsin, USA.
[17] M. C. Burla, M. Camalli, B. Carrozzini, G. L. Cascarano, C. Giacovazzo, G. Polidori and R. Spagna, *J. Appl. Crystallogr.* **2003**, *36*, 1103-1103.
18 (a) G. M. Sheldrick, *Acta Cryst.* **2008**, *A64*, 112-122; (b) G. M. Sheldrick, *Acta Cryst.* **2015**, *C71*, 3-8.

Table S7. Crystal data and structure refinement for compound **3a·PF_6**.

Empirical formula	$C_{36}H_{49}F_6P_3Pt$	
	$[C_{36}H_{49}P_2Pt, F_6P]$	
Formula weight	883.75	
Temperature	193(2) K	
Wavelength	0.71073 Å	
Crystal system	Orthorhombic	
Space group	Pbca	
Unit cell dimensions	a = 16.9493(8) Å	α = 90°.
	b = 18.3544(8) Å	β = 90°.
	c = 47.091(2) Å	γ = 90°.
Volume	14649.7(11) $Å^3$	
Z	16	
Density (calculated)	1.603 Mg/m^3	
Absorption coefficient	4.017 mm^{-1}	
F(000)	7072	
Crystal size	0.230 x 0.180 x 0.150 mm^3	
Theta range for data collection	2.088 to 28.284°.	
Index ranges	-19<=h<=22, -16<=k<=24, -62<=l<=61	
Reflections collected	154736	
Independent reflections	18170 [R(int) = 0.0993]	
Completeness to theta = 25.242°	99.7 %	
Absorption correction	Semi-empirical from equivalents	
Max. and min. transmission	0.7461 and 0.5031	
Refinement method	Full-matrix least-squares on F^2	
Data / restraints / parameters	18170 / 72 / 849	
Goodness-of-fit on F^2	1.007	
Final R indices [I>2sigma(I)]	R1 = 0.0435, wR2 = 0.0977	
R indices (all data)	R1 = 0.0691, wR2 = 0.1100	
Extinction coefficient	n/a	
Largest diff. peak and hole	2.501 and -1.912 e.$Å^{-3}$	

Table S8. Crystal data and structure refinement for compound **3b·BF_4**.

Empirical formula	$C_{35}H_{55}BCl_2F_4P_2Pt$	
	$[C_{34}H_{53}P_2Pt, BF_4, CH_2Cl_2]$	
Formula weight	890.53	
Temperature	193(2) K	
Wavelength	0.71073 Å	
Crystal system	Triclinic	
Space group	$P\bar{1}$	
Unit cell dimensions	a = 11.6490(13) Å	α = 80.709(5)°.
	b = 12.4817(13) Å	β = 86.185(5)°.
	c = 14.4148(15) Å	γ = 68.498(4)°.
Volume	1924.4(4) $Å^3$	
Z	2	
Density (calculated)	1.537 Mg/m^3	
Absorption coefficient	3.910 mm^{-1}	
F(000)	896	
Crystal size	0.250 x 0.150 x 0.050 mm^3	
Theta range for data collection	2.066 to 25.248°.	
Index ranges	-13<=h<=13, -14<=k<=14, -17<=l<=16	
Reflections collected	27700	
Independent reflections	6948 [R(int) = 0.0297]	
Completeness to theta = 25.242°	99.9 %	
Absorption correction	Semi-empirical from equivalents	
Max. and min. transmission	0.7461 and 0.5324	
Refinement method	Full-matrix least-squares on F^2	
Data / restraints / parameters	6948 / 36 / 419	
Goodness-of-fit on F^2	1.039	
Final R indices [I>2sigma(I)]	R1 = 0.0202, wR2 = 0.0510	
R indices (all data)	R1 = 0.0225, wR2 = 0.0518	
Extinction coefficient	n/a	
Largest diff. peak and hole	0.884 and -0.552 e.$Å^{-3}$	

Table S9. Crystal data and structure refinement for compound **3c·BF_4**.

Empirical formula	$C_{34}H_{53}BF_4P_2Pt$	
	$[C_{34}H_{53}P_2Pt, BF_4]$	
Formula weight	805.60	
Temperature	193(2) K	
Wavelength	0.71073 Å	
Crystal system	Monoclinic	
Space group	$P2_1/n$	
Unit cell dimensions	a = 11.8390(12) Å	α = 90°.
	b = 11.7018(10) Å	β = 93.286(5)°.
	c = 24.993(2) Å	γ = 90°.
Volume	3456.7(6) $Å^3$	
Z	4	
Density (calculated)	1.548 Mg/m^3	
Absorption coefficient	4.195 mm^{-1}	
F(000)	1624	
Crystal size	0.200 x 0.150 x 0.100 mm^3	
Theta range for data collection	2.550 to 25.250°.	
Index ranges	-14<=h<=14, -13<=k<=14, -29<=l<=29	
Reflections collected	46412	
Independent reflections	6241 [R(int) = 0.0582]	
Completeness to theta = 25.242°	99.9 %	
Absorption correction	Semi-empirical from equivalents	
Max. and min. transmission	0.9011 and 0.8509	
Refinement method	Full-matrix least-squares on F^2	
Data / restraints / parameters	6241 / 24 / 390	
Goodness-of-fit on F^2	1.017	
Final R indices [I>2sigma(I)]	R1 = 0.0286, wR2 = 0.0747	
R indices (all data)	R1 = 0.0368, wR2 = 0.0784	
Extinction coefficient	n/a	
Largest diff. peak and hole	1.480 and -0.579 e.$Å^{-3}$	

NMR spectra

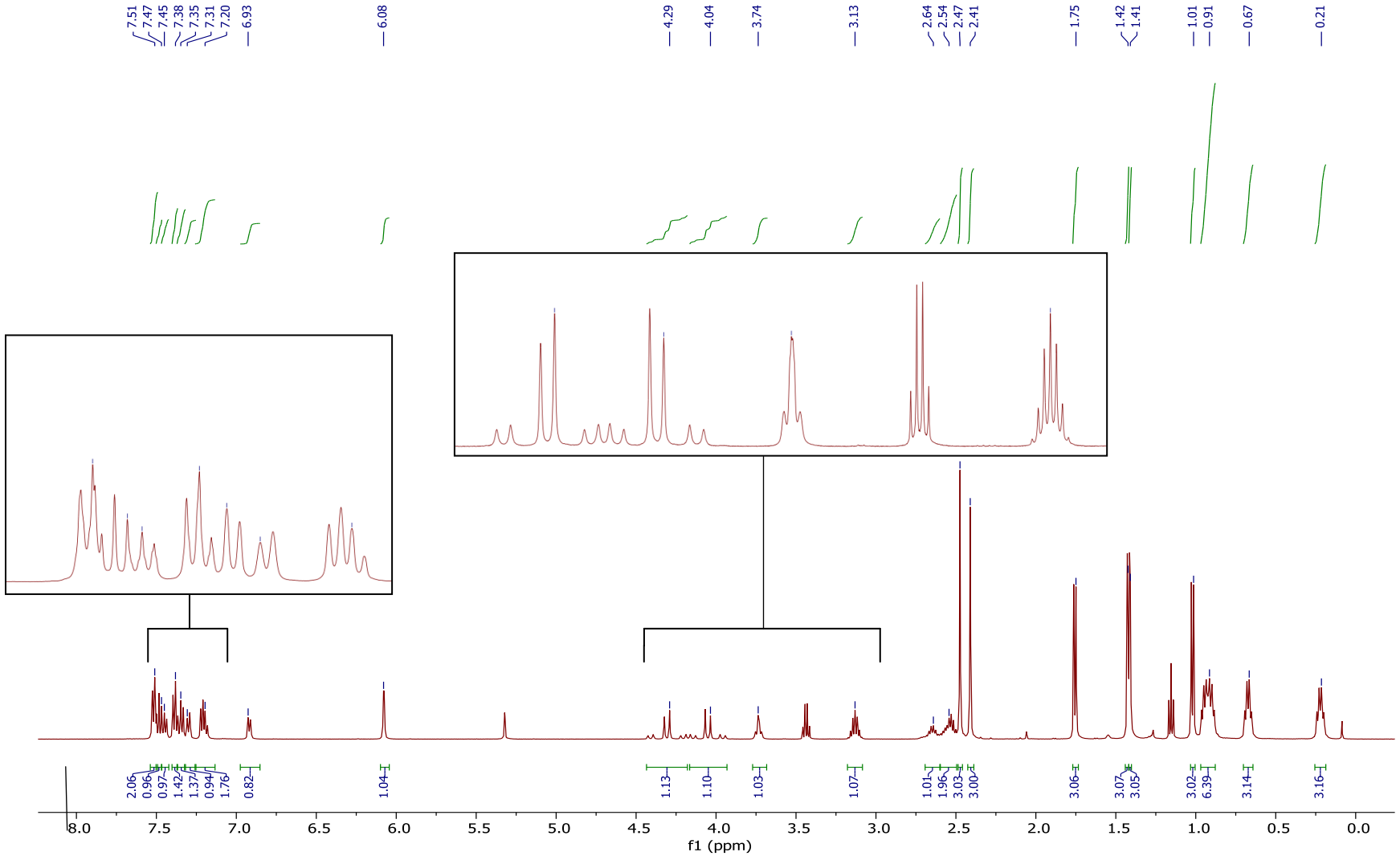

Figure S6. ^{1}H NMR spectrum of complex **3a·PF$_6$** in CD_2Cl_2.

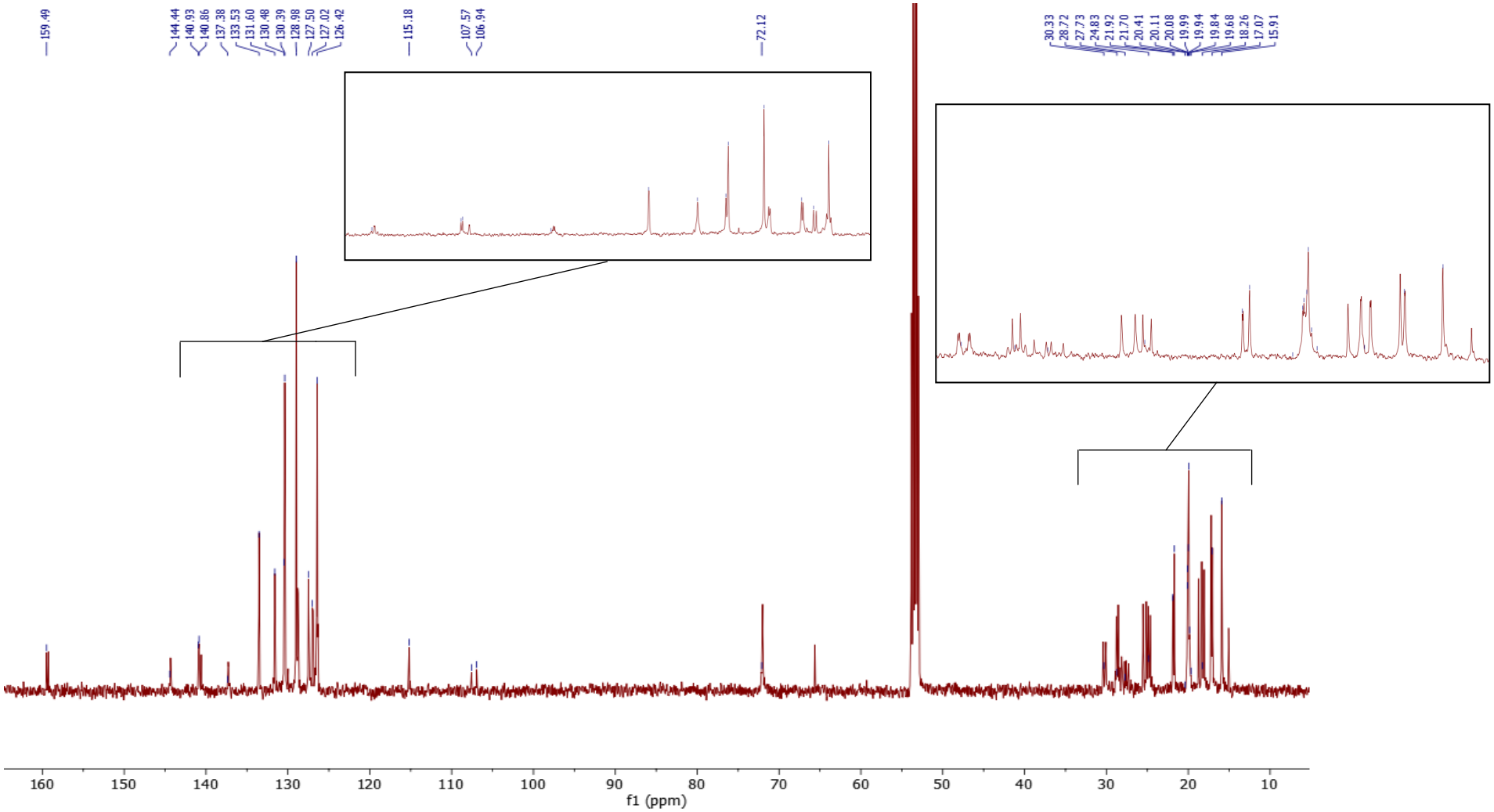

Figure S7. $^{13}C\{^{1}H\}$ NMR spectrum of complex **3a·PF$_6$** in CD_2Cl_2.

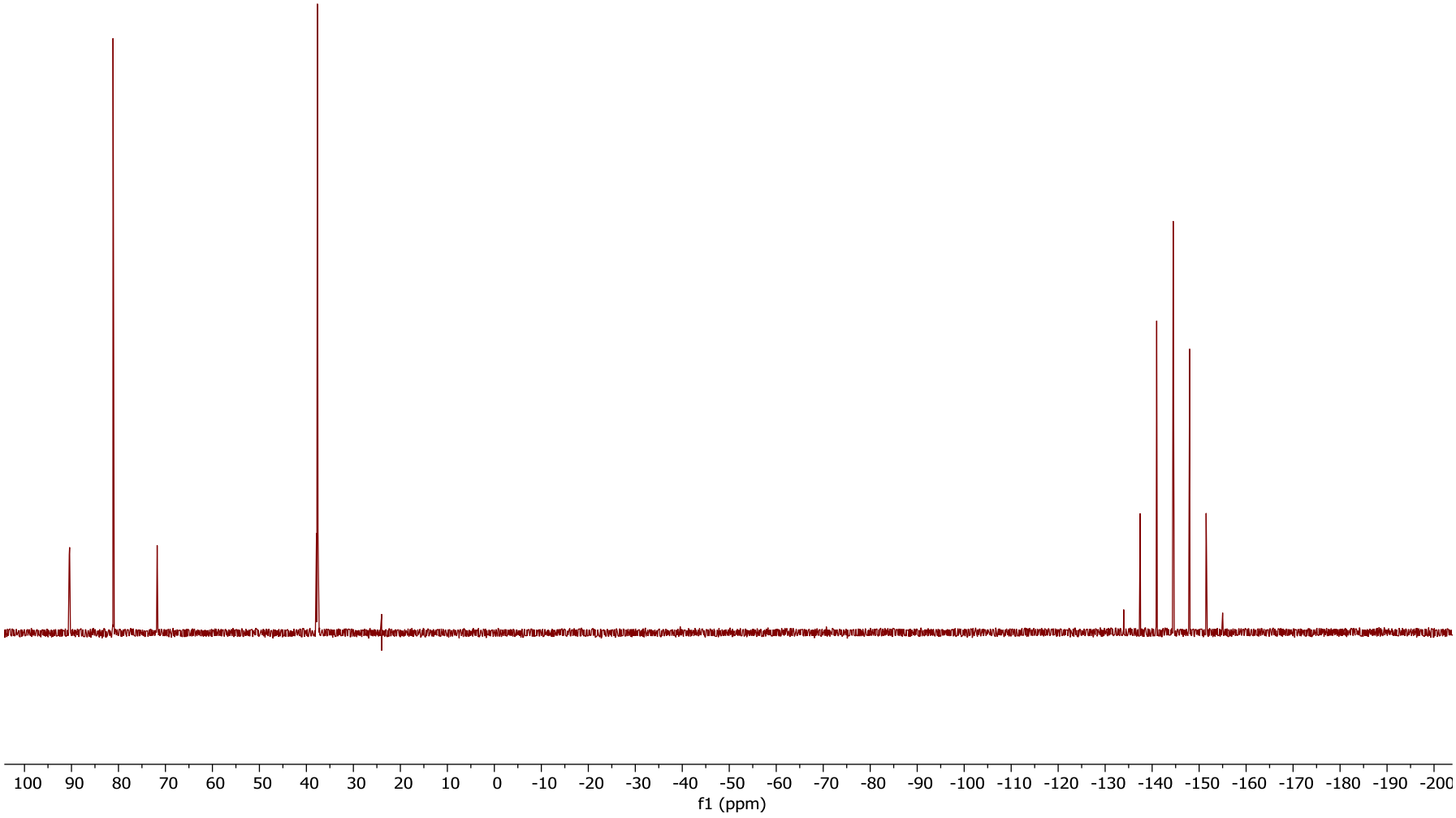

Figure S8. $^{31}P\{^{1}H\}$ NMR spectrum of complex **3a·PF_6** in CD_2Cl_2.

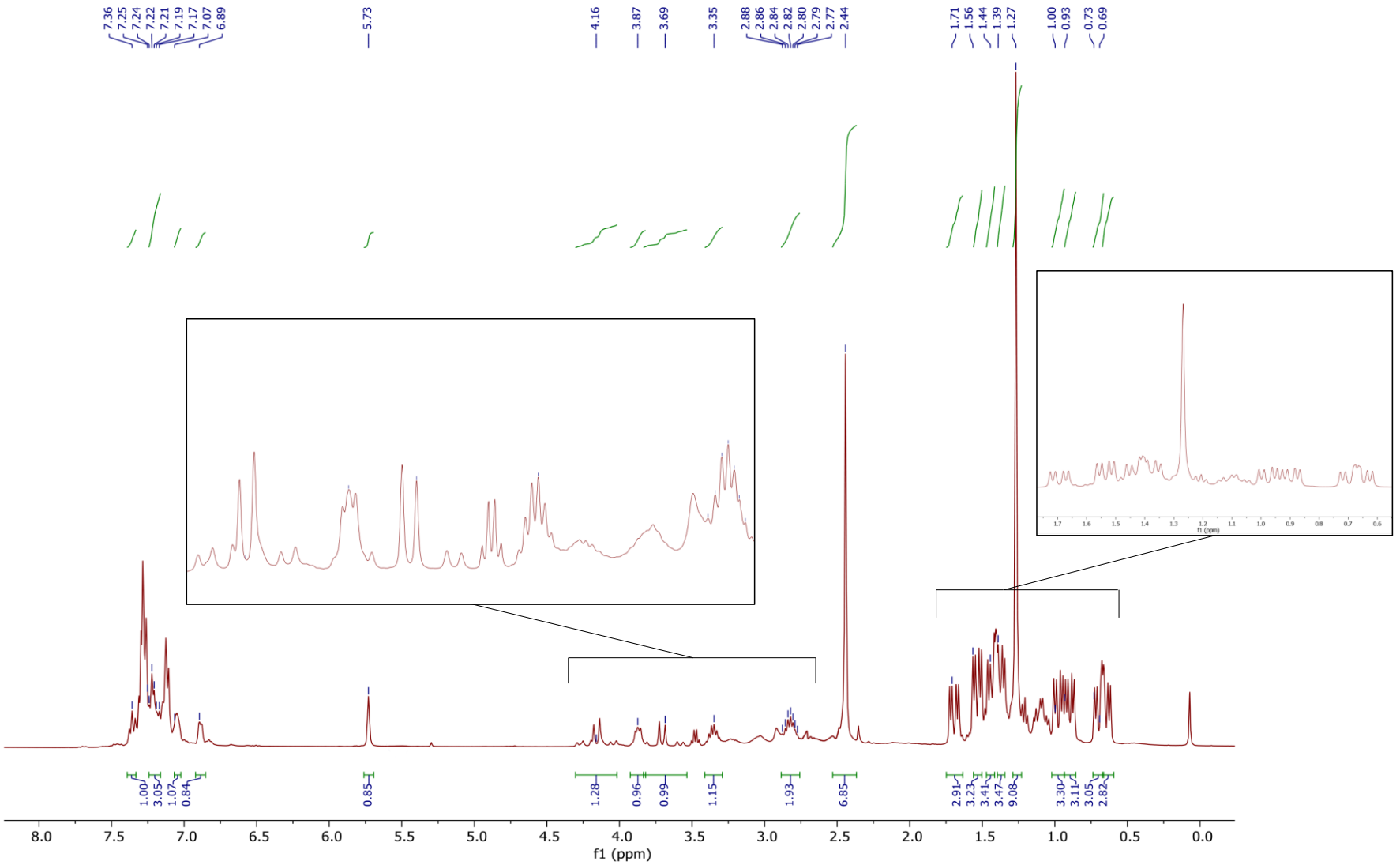

Figure S9. ^{1}H NMR spectrum of complex **3b·BF$_4$** in CD_2Cl_2.

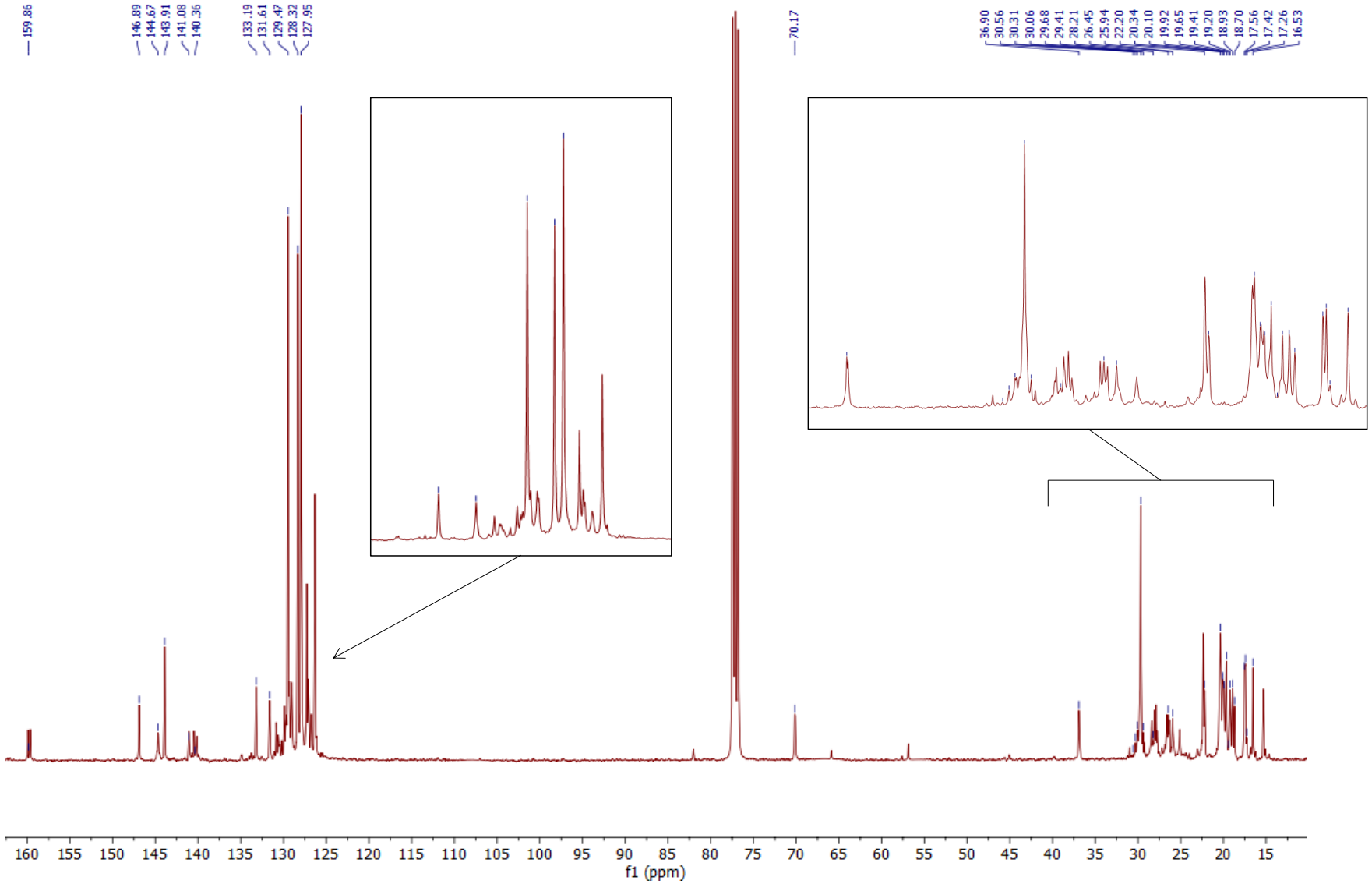

Figure S10. $^{13}C\{^{1}H\}$ NMR spectrum of complex **3b·BF$_4$** in CD_2Cl_2.

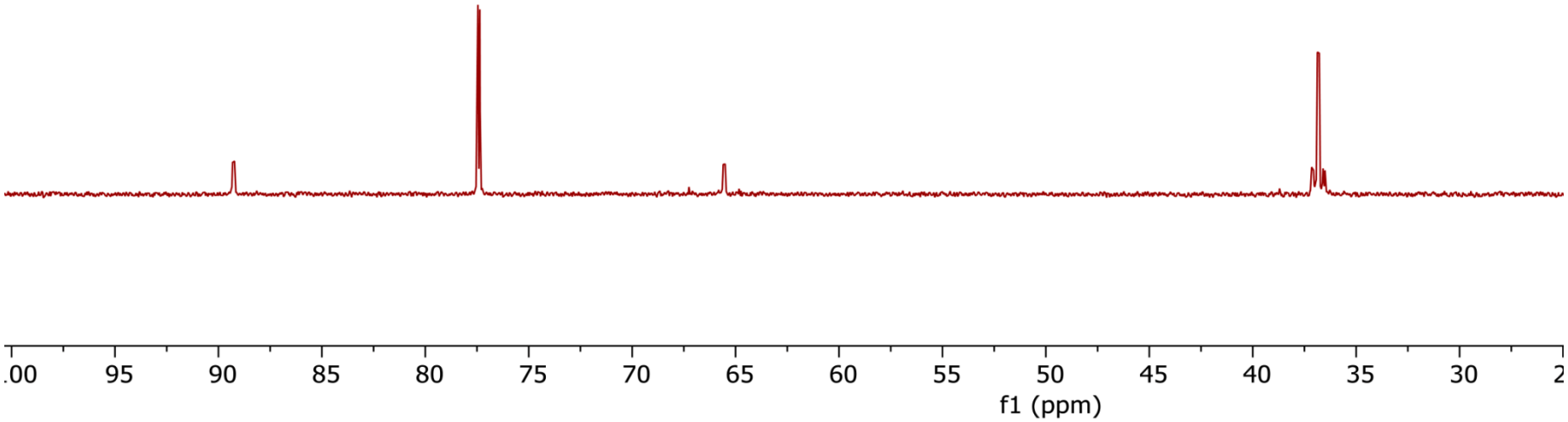

Figure S11. $^{13}C\{^{1}H\}$ NMR spectrum of complex **3b·BF$_4$** in CD_2Cl_2.

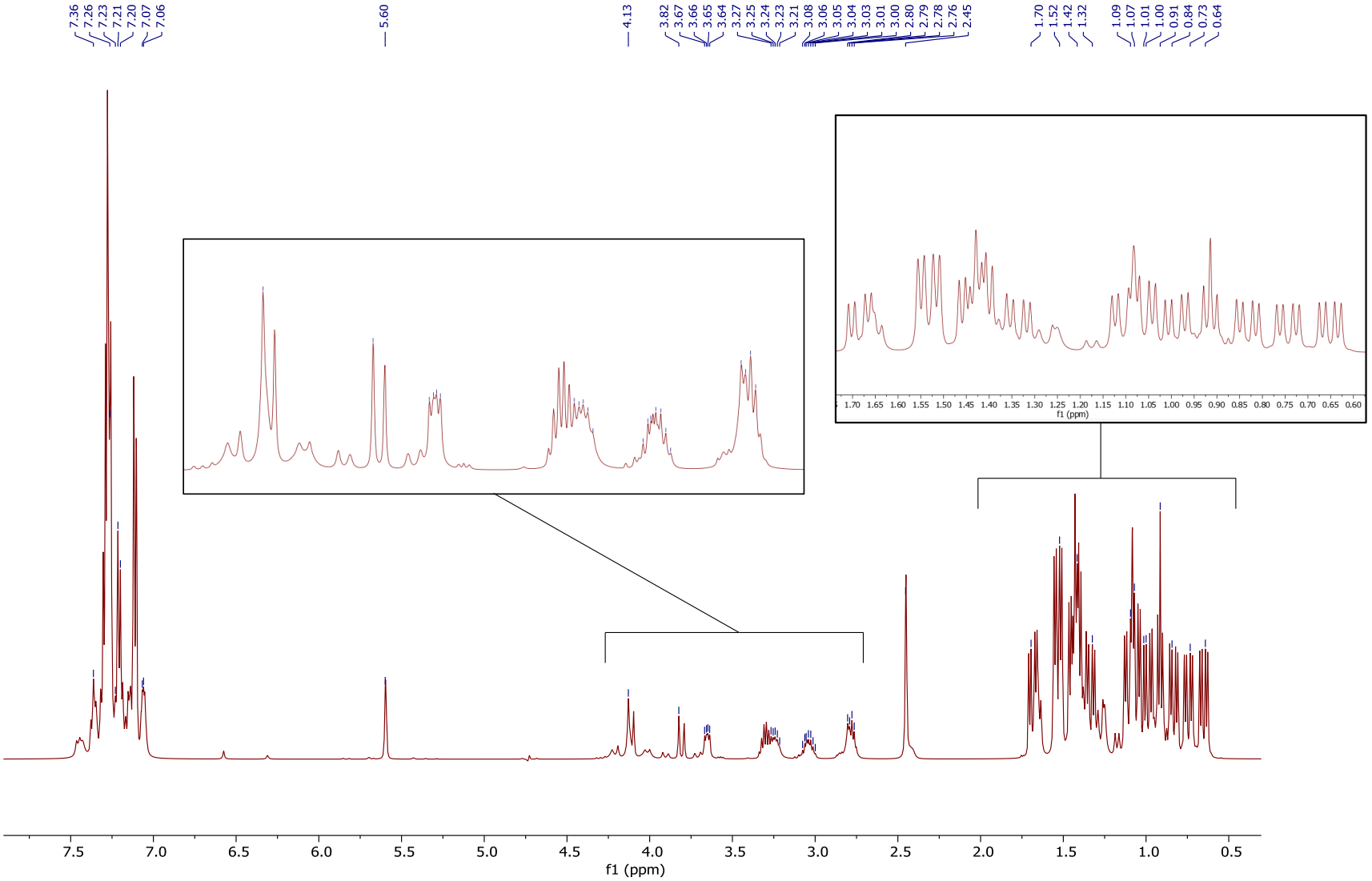

Figure S12. ^{1}H NMR spectrum of complex **3c·BF$_4$** in CD_2Cl_2.

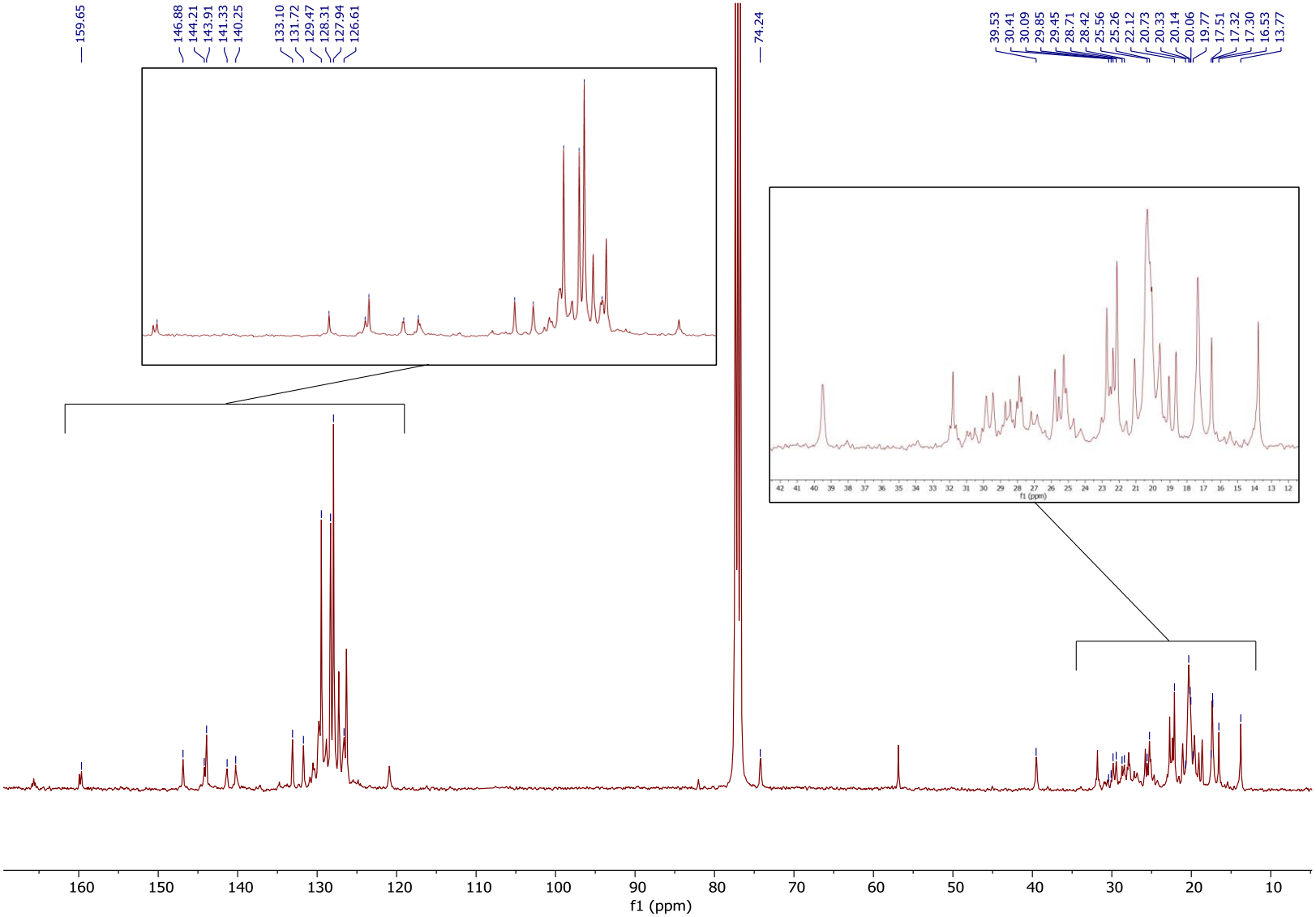

Figure S13. $^{13}C\{^{1}H\}$ NMR spectrum of complex **3c·BF_4** in CD_2Cl_2.

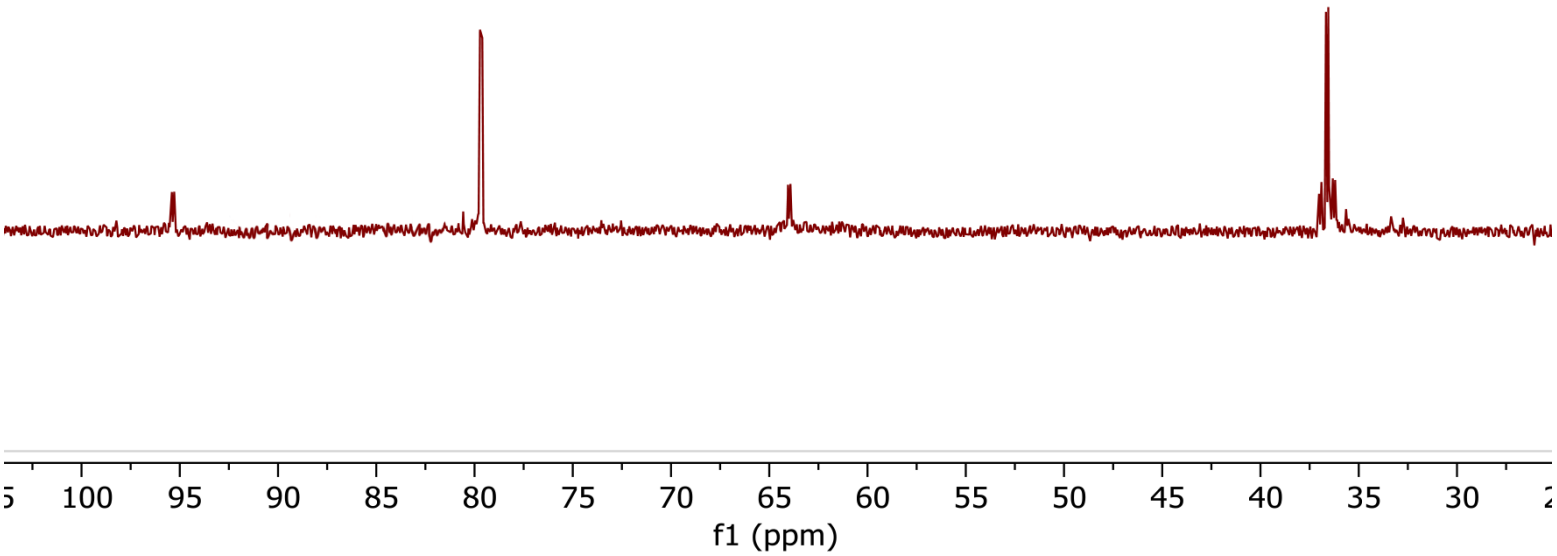

Figure S14. $^{31}P\{^{1}H\}$ NMR spectrum of complex **3c·BF$_4$** in CD_2Cl_2.

References

[1] J. Campos, R. Peloso and E. Carmona, *Angew. Chem. Int. Ed.*, 2012, **51**, 8255-8258.

[2] Gaussian 09, Revisions B.01 and E.01, M. J. Frisch, G. W. Trucks, H. B. Schlegel, G. E. Scuseria, M. A. Robb, J. R. Cheeseman, G. Scalmani, V. Barone, G. A. Petersson, H. Nakatsuji, X. Li, M. Caricato, A. Marenich, J. Bloino, B. G. Janesko, R. Gomperts, B. Mennucci, H. P. Hratchian, J. V. Ortiz, A. F. Izmaylov, J. L. Sonnenberg, D. Williams-Young, F. Ding, F. Lipparini, F. Egidi, J. Goings, B. Peng, A. Petrone, T. Henderson, D. Ranasinghe, V. G. Zakrzewski, J. Gao, N. Rega, G. Zheng, W. Liang, M. Hada, M. Ehara, K. Toyota, R. Fukuda, J. Hasegawa, M. Ishida, T. Nakajima, Y. Honda, O. Kitao, H. Nakai, T. Vreven, K. Throssell, J. A. Montgomery, Jr., J. E. Peralta, F. Ogliaro, M. Bearpark, J. J. Heyd, E. Brothers, K. N. Kudin, V. N. Staroverov, T. Keith, R. Kobayashi, J. Normand, K. Raghavachari, A. Rendell, J. C. Burant, S. S. Iyengar, J. Tomasi, M. Cossi, J. M. Millam, M. Klene, C. Adamo, R. Cammi, J. W. Ochterski, R. L. Martin, K. Morokuma, O. Farkas, J. B. Foresman and D. J. Fox, Gaussian, Inc., Wallingford CT, 2010.

[3] (a) R. Ditchfield, W. J. Hehre and J. A. Pople , *J. Chem. Phys.* **1971**, *54*, 724-728; (b) W. J. Hehre, R. Ditchfield and J. A. Pople *J. Chem. Phys.* **1972**, *56*, 2257-2261; (c) P. C. Hariharan and J. A. Pople, *Theor. Chim. Acta* **1973**, *28*, 213-222; (d) M. M. Francl, W. J. Pietro, W. J. Hehre, J. S. Binkley, M. S. Gordon, D. J. DeFrees and J. A. Pople, *J. Chem. Phys.* **1982**, *77*, 3654-3665.

[4] D. Andrae, U. Haeussermann, M. Dolg, H. Stoll and H. Preuss, *Theor. Chim. Acta* **1990**, *77*, 123-141.

[5] J.-D. Chai and M. Head-Gordon, *Phys. Chem. Chem. Phys.* **2008**, *10*, 6615-6620.

[6] S. Grimme, *J. Comp. Chem* **2006**, *27*, 1787-1799.

[7] A. V. Marenich, C. J. Cramer and D. G. Truhlar, *J. Phys. Chem. B* **2009**, *113*, 6378–6396.

[8] (a) S. F. Boys, *Rev. Mod. Phys.* **1960**, *32*, 296-299; (b) J. M. Foster and S. F. Boys, *Rev. Mod. Phys.* **1960**, *32*, 300-302.

[9] (a) Multiwfn, v. 6.0. http://sobereva.com/multiwfn/; (b) T. Lu and F. Chen, *J. Comput. Chem.* **2012**, *33*, 580-592.

[10] (a) E. D. Glendening, C. R. Landis and F. Weinhold, *J. Comput. Chem.* **2013**, *34*, 1429-1437; (b) E. D. Glendening, J. K. Badenhoop, A. E. Reed, J. E. Carpenter, J. A. Bohmann, C. M. Morales, C. R. Landis and F. Weinhold, NBO 6.0.; Theoretical Chemistry Institute, University of Wisconsin: Madison, **2013**.

[11] C. Y. Legault, CYLview, 1.0b, Université de Sherbrooke, **2009**.

[12] W. Humphrey, A. Dalke and K. Schulten, *J. Molec. Graphics,* **1996**, *14*, 33-38. The VMD software can be downloaded from https://www.ks.uiuc.edu/Research/vmd/.

[13] P. Vidossich and A. Lledós, *Dalton Trans.* **2014**, *43*, 11145-11151.

[14] I. Mayer, *Chem. Phys. Lett.* **1983**, *97*, 270-274.

[15] Bruker. SAINT. *APEX2* **2007**, Bruker AXS Inc., Madison, Wisconsin, USA.

[16] (a) G. M. Sheldrick, SADABS, Programs for Scaling and Absorption Correction of Area Detector Data. *SADABS, Programs Scaling Absorpt. Correct. Area Detect. Data* **1997**, University of Göttingen: Göttingen, Germany; (b) Bruker. SADABS. *APEX2* **2007**, Bruker AXS Inc., Madison, Wisconsin, USA.

[17] M. C. Burla, M. Camalli, B. Carrozzini, G. L. Cascarano, C. Giacovazzo, G. Polidori and R. Spagna, *J. Appl. Crystallogr.* **2003**, *36*, 1103-1103.

[18] (a) G. M. Sheldrick, *Acta Cryst.* **2008**, *A64*, 112-122; (b) G. M. Sheldrick, *Acta Cryst.* **2015**, *C71*, 3-8.